

Thermo-elastoplastic characteristics of heat-resisting functionally graded composite structures

Jin-Rae Cho[†] and Dae-Yul Ha[‡]

School of Mechanical Engineering, Pusan National University, Pusan 609-735, Korea

Abstract. This paper is concerned with a study on thermo-elastoplastic characteristics of functionally graded composite. Compared to the classical layered composites, it shows a wide range of thermo-elastoplastic characteristics according to the choice of two major parameters, the thickness-wise volume fraction of constituents and the relative thickness ratio of the graded layer. Therefore, by selecting an appropriate combination of the two parameters, one is expected to design the most suitable heat-resisting composite for a given thermal circumstance. Here, we address the parametric investigation on its characteristics together with theoretical study on thermo-elastoplasticity and numerical techniques for its finite element approximations. Through the numerical experiments, we examine the influence of two parameters on the thermo-elastoplastic characteristics.

Key words: functionally graded material (FGM); graded layer; volume fraction; relative thickness ratio; material properties; stress concentration; thermo-elastoplastic characteristics.

1. Introduction

Materials for the high-temperature engineering applications are required to possess superior thermo-mechanical performances such as high temperature-strength and creep-resistance, excellent fracture toughness and thermal shock resistance. Since single-composed materials are almost impossible to meet simultaneously such multi-performances, conventional laminated composites (CLC) manufactured by combining metals and ceramics have been successfully used for several decades.

However, owing to the inherent methodology, CLCs possess an inevitable disadvantage, a discontinuity in material composition at layer interfaces. This material discontinuity may lead to sharp kinks in thermal stress distribution, and which may bring stress concentration or cracking near such interfaces. In addition, those may trigger the initiation of plasticization or cracking reaching at unexpected structural failure (Williamson *et al.* 1993, Suresh *et al.* 1995, Tanaka *et al.* 1993, Hirano and Wakashima 1995, Reddy *et al.* 1999, Cho and Oden 2000).

To resolve this problem, a notion of functionally graded materials (FGM) has been introduced in late 1980s. In FGMs, dual-phase heterogeneous layers called the graded layer are included in which a material composition varies continuously from one end to the other. This material technology was initiated originally for the development of heatproof structures of space shuttles (Niino *et al.* 1990).

According to the advancement of manufacturing techniques such as chemical or physical vapor

[†] Assistant Professor

[‡] Graduate Student

deposition, thermal spray and powder metallurgy, active and intensive research activities are currently ongoing for diverse engineering applications to turbo-engines, high-speed tools, automobile engines, and so on. However, an elaborate tailoring of the material composition and the geometry dimension is essential to satisfy the target performance. This is because the success of designed FGMs depends definitely on the suitability of combination of the volume fraction and the relative thickness ratio of the graded layer.

In order to design an optimum heat-resisting FGM, one preliminarily needs to explore the thermo-elastoplastic characteristics with respect to the design parameters. In other words, one needs the parametric analysis to examine the plastic zone and its location, distributions of equivalent plastic strain and thermal stress and so on, for a variety of combinations of the two parameters.

In this paper, we first address the parametric and material characteristics of FGMs together with the fundamental thermo-elastoplasticity theory. Next, we approximate heat diffusion and elastoplastic deformation fields according to the unconditionally stable *Crank-Nicolson-Galerkin* scheme and the incremental numerical technique, respectively. With the introduced finite element approximation scheme we conduct numerical experiments, with a representative two-dimensional beam-like functionally graded structure, in order to investigate the effect of the volume fraction and the relative thickness on the thermo-elastoplastic characteristics.

2. Functionally graded composite structures

Fig. 1 shows a three-dimensional symmetric metal-ceramic FGM composite, where $2d$ and $2d_G$ indicate respectively thickness of the plate and the graded layer. As mentioned earlier, the material composition varies continuously through the thickness such that no discontinuity occurs.

Throughout this paper, we assume that layers are perfectly bonded and initially stress-free. Furthermore, the ceramic layer is linearly elastic while the metal layer obeys linearly elastic rigidplastic behavior. Then, the graded layer becomes a transversely isotropic (with respect to the xy -plane) and linearly elastic rigid-plastic material.

As discussed in our pervious work (Cho and Oden 2000), the thermo-mechanical behavior of FGMs is strongly characterized by two parameters, the relative thickness ratio χ of the graded layer

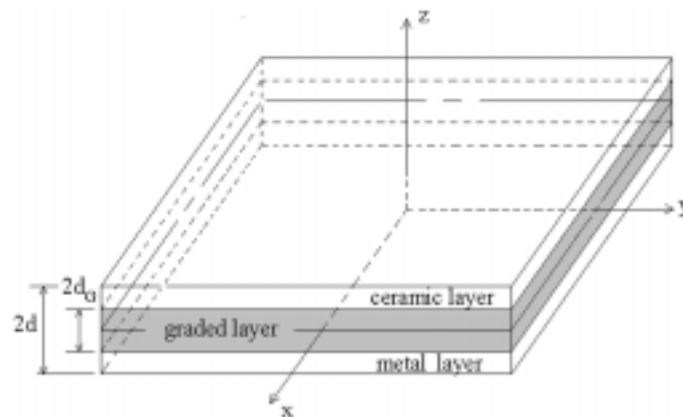


Fig. 1 Three-layered heat resisting functionally graded composite plate

defined by

$$\chi = d_G/d, \quad 0 \leq \chi \leq 1 \quad (1)$$

and the volume fraction functions $V_m(z)$ and $V_c(z)$ of metal and ceramic constituents (here, subscripts m and c refer to metal and ceramic, respectively).

Since two volume-fraction functions satisfy the relation: $V_m+V_c=1$ at every point in FGMs, one needs to define either of the two. Here, we define the volume fraction of the metal such that.

$$V_m(z) = \begin{cases} \left(\frac{d_G-z}{2d_G}\right)^N, & |z| \leq d_G \\ 1, & (-d \leq z \leq -d_G) \\ 0, & d_G \leq z \leq d \end{cases} \quad (2)$$

where power index N are positive real numbers.

As a first step, we consider the characteristics of FGM when two parameters approach lower or upper limits. It is obvious that FGMs approach classical layered composites (CLC) AS χ tends to zero while *full FGMs* (f-FGMs) as χ tends to unity.

On the other hand, the graded layer becomes to be dominated by metal or ceramic compound when the power index in V_m approaches 0 or $+\infty$, as illustrated in Fig. 2. In this paper, we denote a FGM dominated by metal layer as the *metal layer-extended CLC* (m-CLC) while one dominated by ceramic layer as the *ceramic layer-extended CLC* (c-CLC), respectively.

According to the two parameters, we construct two different families of FGMs. First, for a given power index $N(0 < N < +\infty)$, the χ -family F_χ is defined as a set of infinite FGMs that are sequentially distinguished by the choice of relative thickness ratio:

$$F_\chi = \{M_N^\chi: M_N^0 = CLC, M_N^1 = f-FGM, 0 \leq \chi \leq 1\} \quad (3)$$

Similarly, the N -family F_N is constructed by sequentially varying the power index, for a fixed relative thickness ratio χ ($0 < \chi \leq 1$):

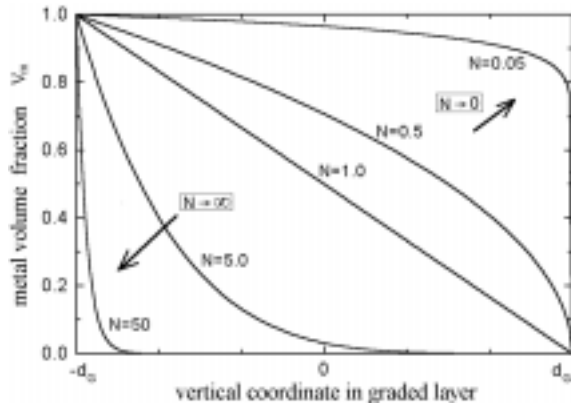


Fig. 2 Metal volume fraction functions in the graded layer for different N

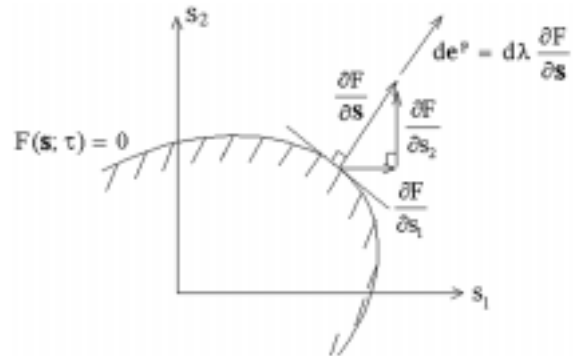


Fig. 3 Normality principle and Prandtl-Reuss relations

$$F_N = \{M_\chi^N : M_\chi^0 = m - CLC, M_\chi^{+\infty} = c - CLC, 0 \leq q + \infty\} \quad (4)$$

The purpose of such FGM families is to examine sort of sequential variations in thermo-elastoplastic characteristics along the two defined parameters. In this study, our concerns focus on the size and location of plastic zones and the distributions of thermal stresses and plastic strains caused by cyclic heating.

3. Theory and material properties

3.1. Thermo-elastoplasticity theory

When a state of stresses at a point in FGM composites reaches at a critical level, yielding starts from that point. A condition for yielding is expressed by the generalized yield surface

$$\left. \begin{aligned} F(s, \tau) = f(s) - k^2(\tau) = 0 \\ k(\tau) = k(\bar{\epsilon}_p; T) = k_0(\bar{\epsilon}_p) - k_1(T) \end{aligned} \right\} \quad (5)$$

where s and $\bar{\epsilon}_p$ denote a deviatoric stress tensor of *Cauchy* stresses $\sigma (s_{ij} = \sigma_{ij} - \theta \delta_{ij}, \theta = \sigma_{kk}/3)$, and the equivalent plastic strain, respectively. And, τ is the work-hardening parameter.

For our study we assume that FGMs obey isotropic hardening rule and von-Mises yield criterion:

$$\left. \begin{aligned} f(s) = J_2 = \frac{1}{2} s : s \\ k(\tau) = \sigma_Y / \sqrt{3} \end{aligned} \right\} \quad (6)$$

with $\sigma_Y = \sigma_Y(\bar{\epsilon}_p; T)$ indicating yield stress in uniaxial tension. Furthermore, we employ *Prandtl-Reuss* equations for increments of plastic strains given by

$$de^p = d\lambda \frac{\partial F}{\partial s}, d\lambda \sim \text{a scalar multiplier} \quad (7)$$

where e^p is deviatoric strain tensor of plastic deformation. Assuming no creep, the total increment of deviatoric strain is sum of elastic and plastic strain increments,

$$de = de^e + de^p \quad (8)$$

where $e_{ij} = \epsilon_{ij} - \Delta \delta_{ij}/3$, $\Delta = \epsilon_{kk}$. Taking total differentiation to the yield surface function, we have

$$dF = \frac{\partial F}{\partial s} : ds + \frac{\partial F}{\partial e^p} : de^p + \frac{\partial F}{\partial T} dT = 0 \quad (9)$$

$$d\lambda = -\frac{1}{A} \left(\frac{\partial F}{\partial s} : ds + \frac{\partial F}{\partial T} dT \right), A = \frac{\partial F}{\partial s} : \frac{\partial F}{\partial e^p} \quad (10)$$

Furthermore, we obtain

$$\frac{\partial F}{\partial s} = \frac{\partial J_2}{\partial s} = s \quad (11)$$

$$\frac{\partial F}{\partial T} = 2k \frac{dk_1}{dT} = 2\beta\sqrt{J_2}, \quad \beta = \frac{dk_1}{dT} = -\frac{d\sigma_Y}{\sqrt{3}dT} \quad (12)$$

in this paper, β is assumed to be temperature-interval-wise constant satisfying

$$\beta = \begin{cases} c, & \Delta T > 0 \\ 0, & \Delta T \leq 0 \end{cases}, \quad c \sim \text{const} \quad (13)$$

Using Eqs. (11) and (12), we have

$$\left. \begin{aligned} d\lambda &= -\frac{1}{A}(s:ds + 2\beta\sqrt{J_2}dT) \\ de^p &= s d\lambda \end{aligned} \right\} \quad (14)$$

Next, we record basic relations:

$$\left. \begin{aligned} \bar{\sigma} &= \sqrt{\frac{3}{2}s:s} = \sqrt{3J_2} \\ d\bar{\sigma} &= \sqrt{3/2} \cdot \frac{s:ds}{\sqrt{s:s}} = \sqrt{\frac{3}{4J_2}} \cdot s:ds \\ \bar{\sigma} d\bar{\sigma} &= \frac{3}{2}s:ds \end{aligned} \right\} \quad (15)$$

Substituting Eq. (15) into (14), we have the relation between equivalent stress and equivalent plastic strain given by

$$d\bar{\epsilon}_p = -\frac{2\bar{\sigma}}{3A} \left[\frac{2}{3}\bar{\sigma}d\bar{\sigma} + \frac{2}{\sqrt{3}}\beta\bar{\sigma}dT \right] \quad (16)$$

Fig. 4 depicts the elastoplastic tangent modulus E_T and the plastic modulus H defined by

$$H(\bar{\epsilon}_p; T) = \frac{\partial \bar{\sigma}}{\partial \bar{\epsilon}_p} = \frac{EE_T}{E - E_T} \quad (17)$$

Substituting the relation $\bar{\sigma} = \sqrt{3}[k_0(\bar{\epsilon}_p) - k_1(T)]$ obtained from Eqs. (5), (7) and (10) into Eq. (17), we have

$$d\bar{\epsilon}_p = \sqrt{3} \cdot \frac{dk_0}{H} = \frac{1}{H}(d\bar{\sigma} + \sqrt{3}\beta dT) \quad (18)$$

Equating Eq. (16) to Eq. (18) leads to

$$\begin{aligned} A &= -\frac{2}{9}H\bar{\sigma}^2 \\ d\lambda &= \frac{3}{2H\bar{\sigma}}(d\bar{\sigma} + \sqrt{3}\beta dT) \end{aligned} \quad (19)$$

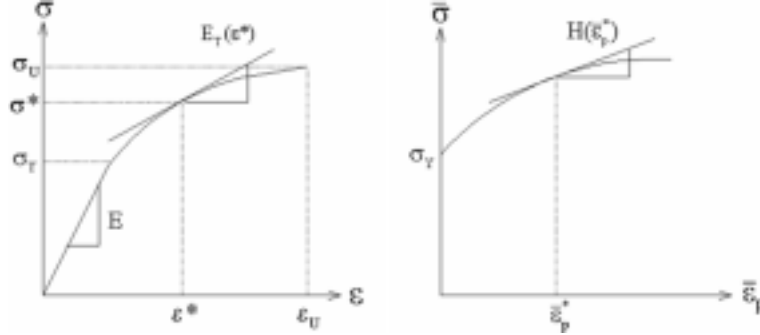


Fig. 4 Elastoplastic and plastic moduli for elastic work-hardening materials

$$de^p = \frac{3s}{2H\bar{\sigma}}(d\bar{\sigma} + \sqrt{3}\beta dT) \quad (20)$$

From the basic relation of $de = ds/2G + de^p$ (G ~the shear modulus) together with Eqs. (15) and (20), we have

$$s:de = \frac{\bar{\sigma}d\bar{\sigma}}{3G} + \frac{2}{3}\bar{\sigma}^2 d\lambda \quad (21)$$

Substitution $d\bar{\sigma}$ in Eq. (19) into the above relation, we arrive at

$$s:de = Sd\lambda - QdT \quad (22)$$

with

$$S = \frac{2\bar{\sigma}^2}{9G}(H + 3G), \quad Q = \frac{\beta\bar{\sigma}}{\sqrt{3}G} \quad (23)$$

Prandtl-Reuss equations, together with $s_{kk}=0$, imply the incompressible plastic deformation: $d\Delta = \lambda s_{kk}=0$. Hence, we can use the basic relation

$$d\theta = (d\Delta - 3\alpha dT)K \quad (24)$$

where $K(=\lambda+2G/3)$ is the bulk modulus.

Now, we construct the relation for stress increments using the relations established so far,

$$\begin{aligned} d\sigma &= ds + \mathbf{1}d\theta \\ &= 2G(de - de^p) + \mathbf{1}d\theta \\ &= 2G\left[de - sd\lambda - \frac{Q}{S}s dT\right] + \mathbf{1}d\theta \\ &= 2G\left[de - s(s:de/S) - \frac{Q}{S}s dT\right] + (d\Delta - 3\alpha dT)\mathbf{1}K \end{aligned} \quad (25)$$

where $\mathbf{1}$ denotes $\{1, 1, 1, 0, 0, 0\}^T$. It is worthy noting that we apply $(\partial F/\partial s=s)$ to the second step. From the relations of material moduli of linearly elastic materials, we have

$$2Gde + d\Delta 1K = D_e d\varepsilon \quad (26)$$

with D_e defined as a (6×6) elastic material matrix defining *Cauchy* strains.

By defining the plastic material matrix D_p and the elastoplastic material matrix D_{ep} , respectively, by

$$\left. \begin{aligned} D_p &= \frac{2G}{S} s s^T \\ D_{ep} &= (D_e - D_p) \end{aligned} \right\} \quad (27)$$

we finally obtain the constitutive law for thermo-elastoplastic materials (with $s:de+s:d\varepsilon$):

$$d\sigma = D_{ep} d\varepsilon - D_e \alpha dT - 2G \frac{Q}{S} s dT \quad (28)$$

where a vector α is 1α . The second term in the RHS of Eq. (28) represents a change of normal stresses due to temperature variation while the third term reflects the effect of yield surface contraction due to the temperature increase. Here, D_p and the third term vanish before an initial yielding.

For the two-dimensional plane-stress FGM composites, we can rewrite the above relation into the following form by splitting in-plane (denoted by n) and transverse (denoted by r) parts:

$$\begin{Bmatrix} d\sigma^n \\ d\sigma^r \end{Bmatrix} = \begin{bmatrix} D_{ep}^{nn} & D_{ep}^{nr} \\ D_{ep}^{rn} & D_{ep}^{rr} \end{bmatrix} \begin{Bmatrix} d\varepsilon^n \\ d\varepsilon^r \end{Bmatrix} - \begin{bmatrix} D_e^{nn} & D_e^{nr} \\ D_e^{rn} & D_e^{rr} \end{bmatrix} \begin{Bmatrix} \alpha^n \\ \alpha^r \end{Bmatrix} dT - 2G \frac{Q}{S} \begin{Bmatrix} s^n \\ s^r \end{Bmatrix} dT \quad (29)$$

where in-plane and transverse stress and strain vectors are arranged as $\{a_x, a_y, a_{xy}\}^T$ and $\{a_z, a_{yz}, a_{zx}\}^T$, respectively, and furthermore $\alpha^n = \{1, 1, 0\}^T$ and $\alpha^r = \{1, 0, 0\}^T$. Then, using the condition $d\sigma^r = 0$ and the static condensation technique, we finally obtain

$$\begin{aligned} d\sigma^n &= (D_{ep}^{nn} - D_{ep}^{nr} D_{ep}^{rr^{-1}} D_{ep}^{rn}) d\varepsilon^n - 2G \frac{Q}{S} (s^n - D_{ep}^{nr^{-1}} s^r) dT \\ &\quad - \{ (D_e^{nn} - D_e^{nr^{-1}} D_e^{rn}) \alpha^n + (D_e^{nr} - D_e^{rr^{-1}} D_e^{rr}) \alpha^r \} dT \end{aligned} \quad (30)$$

3.2. Material properties of the graded layer

As being a dual-phase composite material, thermo-mechanical properties of the graded layer are influenced by the shape and size and the dispersion structure of constituents as well as the volume fraction. Numerous investigators have proposed estimation approaches for material properties of dual-phase composites. The reader may refer to Christensen (1979), Wakashima and Tsukamoto (1991), Ravichandran (1994), Reiter and Dvorak (1998) and Cho and Ha (2000) for the detailed discussion on the representative approaches.

For our study, we basically employ the rules of mixtures, and we select Al_2O_3 for the ceramic layer and Ni for the metal layer. Furthermore, we assume that all materials properties except for the coefficient of thermal expansion α , the yield stress σ_Y , the ultimate stress σ_U and strain ε_U , are temperature independent.

The rules of mixtures are simple estimates expressed in a linear combination of the volume fractions and material properties of two constituents. Therefore, the complex influences of the

above-mentioned factors are not taken into consideration. Basically, there are two estimates in the rules of mixtures, the linear and the modified rule of mixtures.

According to the linear rule of mixtures, any material property \wp at a point \mathbf{x} in dual-phase materials is computed through

$$\wp(\mathbf{x}) = V_A(\mathbf{x}) \wp_A(\mathbf{x}) + V_B(\mathbf{x}) \wp_B(\mathbf{x}) \quad (31)$$

where subscripts A and B refer to constituents A and B . The density ρ , the specific heat c , the thermal conductivity κ , the thermal expansion coefficient α and the *Poisson's* ratio ν are estimated by this approach. A use of the linear rule of mixtures for the density is unquestionable and the justification of it for the thermal expansion coefficient has been made by Schapery (1968).

On the other hand, for the *Young's* modulus E , the yield stress σ_Y and the elastoplastic tangent modulus E_T , we employ the modified rule of mixtures proposed by Tamura *et al.* (1976) which has been subsequently adopted by many other investigators. The modified rule of mixtures treats each sublayer in the graded layer as an isotropic one, for which uniaxial stress σ and strain ε are expressed in terms of the average stresses and strains of two constituents and the volume fractions

$$\sigma = \sigma_A V_A + \sigma_B V_B, \quad \varepsilon = \varepsilon_A V_A + \varepsilon_B V_B \quad (32)$$

together with the stress to strain transfer ration q defined by

$$q = (\sigma_A - \sigma_B) / (\varepsilon_A - \varepsilon_B), \quad 0 < q < +\infty \quad (33)$$

Substituting the relation (33) into Eq. (32), we have the expression for the *Young's* modulus :

$$E = \left[V_m E_m \left(\frac{q + E_c}{q + E_m} \right) + (1 - V_m) E_c \right] / \left[V_m \left(\frac{q + E_c}{q + E_m} \right) + (1 - V_m) \right] \quad (34)$$

From the experiment with dual-phase steels by Suresh *et al.* (1995), it has been reported that q of 4.5 Gpa is suitable for arbitrary two-phase materials for a wide range of volume fractions. A schematic representation of the expression (34) is shown in Fig. 5. Reminding the fact of linear elastic behavior of Al_2O_3 layer and using Eq. (32), the yield stress of the graded layer is determined by

$$\sigma_Y = V_m \sigma_{Ym} + (1 - V_m) \sigma_c = \sigma_{Ym} \left\{ V_m + (1 - V_m) \frac{E_c (q + E_m)}{E_m (q + E_c)} \right\} \quad (35)$$

Along the similar procedure, we have the elastoplastic tangent modulus given by

$$E_T = \left[V_m E_{Tm} \left(\frac{q + E_c}{q + E_{Tm}} \right) + (1 - V_m) E_c \right] / \left[V_m \left(\frac{q + E_c}{q + E_{Tm}} \right) + (1 - V_m) \right] \quad (36)$$

According to the temperature-dependence of σ_Y , σ_U and ε_U , E_{Tm} and E_T also vary with the temperature, and E_{Tm} of the rigid-plastic materials is determined if E_m , σ_Y , σ_U and ε_U are given.

4. Finite element approximations

The thermo-elastoplastic behavior of heat-resisting FGMs is governed by two sets of field equations, the heat diffusion equation and the static equilibrium equations. Under the assumption of infinitesimal deformation, two field equations are weakly coupled.

As is well known, the heat diffusion equation is expressed by the following initial-boundary-value

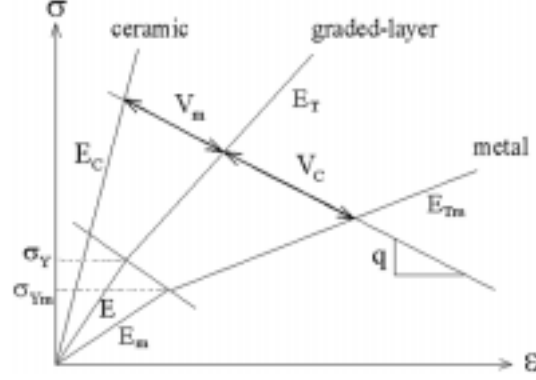


Fig. 5 Schematic representation of the Young's modulus and the elastoplastic tangent modulus according to the modified rule of mixtures

problem, within the spatial domain $x \in \Omega$ during the time interval $t \in (0, t^*]$, such that

$$\left. \begin{aligned} \nabla \cdot (\kappa \nabla T) + q &= \rho c \dot{T}, \quad \text{in } (0, t^*] \times \Omega \\ T &= T_0, \quad \text{at } t = 0 \\ T &= T_0, \quad \text{on } z = +d (0 < t \leq t^*) \\ T &= f(t), \quad \text{on } z = -d (0 < t \leq t^*) \end{aligned} \right\} \quad (37)$$

Here, q denotes an internal heat source and $f(t)$ is a cyclic heating of the period t_p imposed on the upper surface, as shown in Fig. 6.

For the temporal discretization, we make N uniform time partitions such that $\Delta t = t^*/N$, $t^{k+1} = t^k + \Delta t$ ($k=0, 1, \dots, N-1$), and we employ the *Crank-Nicolson scheme* for $T^{k+1/2}$ and $\dot{T}^{k+1/2}$. On the other hand, we define the two scalar-function spaces $V(\Omega)$ and $\tilde{V}(\Omega)$ for test and trial temperature fields, respectively

$$\left. \begin{aligned} V(\Omega) &= \{Q : Q \in H^1(\Omega) \mid \gamma_D Q = 0\} \\ \tilde{V}(\Omega) &= V(\Omega) + \{w_n\} \end{aligned} \right\} \quad (38)$$

where $\gamma_D: H^1(\Omega) \rightarrow H^{1/2}(\partial\Omega)$ denotes a trace operator while $\{w_n\}$ are extended H^1 functions satisfying $w_n|_{z=-d} = T_0$ and $w_n|_{z=d} = f(t_n)$.

Then, we have the following semi-discrete variational formulation for the temperature field by assuming no internal heat source: For a given $T^{k-1} \in \tilde{V}_{k-1}(\Omega)$, find $\Delta T^k(x) \in V(\Omega) + \{\Delta w_k\}$ such that ($k=1, \dots, N$)

$$\int_{\Omega} \left\{ \rho c \Delta T^k Q + \frac{\Delta t}{2} \kappa \nabla(\Delta T^k) \cdot \nabla Q \right\} d\Omega = -\Delta t \int_{\Omega} \kappa \nabla T^{k-1} \cdot \nabla Q d\Omega, \quad \forall Q \in V(\Omega) \quad (39)$$

Now, we partition Ω into a finite number of elements Ω_K with boundaries $\partial\Omega_K$, and we define finite element approximation spaces $V^h(\Omega)$ and $\{w_k\}^h$ with the element-wise continuous basis functions $\{\varphi_i(x)\}_{i=1}^N$ such that

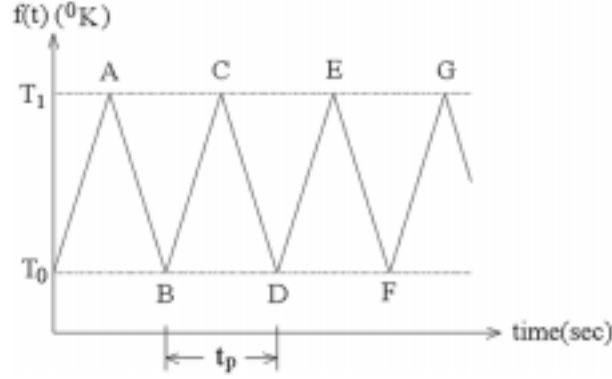


Fig. 6 A cyclic temperature function $f(t)$ of the period t_p

$$V^h(\Omega) \ni Q^h = \sum_{i=1}^N Q_i^h \varphi_i(\mathbf{x}), \quad \{w_k\}^h \ni w_k^h = \sum_{i=1}^N f_i(t_k) \varphi_i(\mathbf{x}) \quad (40)$$

Substituting the finite element approximations into the variational form (39), we arrive at the well-known *Crank-Nicolson-Galerkin* scheme for the successive simultaneous linear equations:

$$\left[C + \frac{\Delta t}{2} \mathbf{K} \right] \Delta \mathbf{T}^k = -\Delta t [\mathbf{K}] \mathbf{T}^{k-1}, \quad k=1, \dots, N \quad (41)$$

Two matrices (time-invariant for FGMs with temperature-independent material properties) are defined by, respectively

$$[C_{ij}] = \int_{\Omega} \rho c \varphi_i \varphi_j d\Omega, \quad [K_{ij}] = \int_{\Omega} \kappa \nabla \varphi_i \cdot \nabla \varphi_j d\Omega \quad (42)$$

For the stability and convergence analysis of this scheme, the reader may refer to Johnson (1990) and Carey and Oden (1984).

Neglecting body force of FGMs, the thermal-induced elastoplastic deformation is governed by the following equilibrium equations

$$\left. \begin{aligned} \sigma_{ij}(u)_{,j} &= 0, \quad \text{in } \Omega \\ u_i &= 0, \quad \text{on } \partial\Omega_D \\ t_i &= 0, \quad \text{on } \partial\Omega_N \end{aligned} \right\} \quad (43)$$

and the displacement-strain relations and the constitutive law

$$2\varepsilon_{ij} = (u_{i,j} + u_{j,i}) \quad (44)$$

$$d\sigma = \mathbf{D}_{ep} d\varepsilon - \mathbf{D}_e \alpha dT - 2G \frac{Q}{S} s dT \quad (45)$$

In Eq. (43), $t_i \in L^2(\partial\Omega_N)$ and n_j denote components of applied external traction and outward unit normal, respectively. We define a vector-valued function space $V(\Omega)$ of admissible displacement fields as

$$V(\Omega) = \{ \mathbf{v}(\mathbf{x}) \in [H^1(\Omega)]^3 \mid \gamma_D \mathbf{v} = \mathbf{0} \} \quad (46)$$

For the iterative numerical analysis, we express the constitutive law as follows:

$$\boldsymbol{\sigma} = \mathbf{D}_{ep} \boldsymbol{\varepsilon} + \boldsymbol{\sigma}^I, \quad \boldsymbol{\sigma}^I = -\mathbf{D}_e \alpha T - 2G \frac{Q}{S} s T \quad (47)$$

Then, we have a nonlinear variational formulation of the boundary value problem (43): Find $\mathbf{u} \in V(\Omega)$ such that, $\forall \mathbf{v} \in V(\Omega)$

$$\int_{\Omega} \boldsymbol{\varepsilon}(\mathbf{v}) : [\mathbf{D}_{ep} \boldsymbol{\varepsilon}(\mathbf{u})] d\Omega = - \int_{\Omega} \boldsymbol{\varepsilon}(\mathbf{v}) : \boldsymbol{\sigma}^I(\mathbf{u}) d\Omega \quad (48)$$

Along the similar procedure for the heat diffusion problem, we construct finite element approximations \mathbf{v}^h of \mathbf{v} such that

$$\left. \begin{aligned} V^h(\Omega) \ni \mathbf{v}^h, \quad v_i^h = \sum_{k=1}^N \bar{v}_k \phi_k(\mathbf{x}) \\ V^h(\Omega) = V(\Omega) \cap [C^0(\bar{\Omega})]^3 \end{aligned} \right\} \quad (49)$$

Employing matrix form expression for \mathbf{v}^h , we have

$$\boldsymbol{\varepsilon}(\mathbf{v}^h) = \mathbf{D}_e (\boldsymbol{\Phi} \bar{\mathbf{v}}) = \mathbf{B} \bar{\mathbf{v}} \quad (50)$$

where $\boldsymbol{\Phi}$ and $\bar{\mathbf{v}}$ indicate the matrix containing finite element basis functions and the nodal vector of \mathbf{v}^h , respectively. Then, we obtain the nonlinear simultaneous equations:

$$\mathbf{K}_{ep} \bar{\mathbf{u}} = \mathbf{f} \quad (51)$$

with

$$\mathbf{K}_{ep} = \int_{\Omega} \mathbf{B}^T \mathbf{D}_{ep} \mathbf{B} d\Omega, \quad \mathbf{f} = - \int_{\Omega} \mathbf{B}^T \boldsymbol{\sigma}^I d\Omega \quad (52)$$

For the iterative finite element analysis, let us introduce a residual force vector \mathfrak{R} defined by

$$\mathfrak{R} = \mathbf{K}_{ep} \bar{\mathbf{u}} - \mathbf{f} \quad (53)$$

In accordance with the *Crank-Nicolson-Galerkin* scheme for successive increments of temperature field ΔT^k , we employ the linearized incremental procedure for the increments $\Delta \bar{\mathbf{u}}^k$:

$$\Delta \mathfrak{R}^k = \mathbf{0}: \quad \mathbf{K}_{ep}^{k-1} \Delta \bar{\mathbf{u}}^k = \Delta \mathbf{f}^k \quad (54)$$

Since we assume that FGMs are linearly isotropic work-hardening materials, we use \mathbf{D}_{ep}^{k-1} , Q^{k-1} , S^{k-1} and s^{k-1} computed at the previous stage $k-1$ for the current-stage computation. With the computed increment $\Delta \mathbf{u}^k$, we calculate $\Delta \boldsymbol{\varepsilon}^k$, $\Delta \boldsymbol{\sigma}^{I(k)}$ and update thermo-elastoplastic stress according to

$$\Delta \boldsymbol{\sigma}^k = \mathbf{D}_{ep}^{k-1} \Delta \boldsymbol{\varepsilon}^k + \Delta \boldsymbol{\sigma}^{I(k)}, \quad \Delta \boldsymbol{\sigma}^{I(k)} = -\mathbf{D}_e \alpha \Delta T^k - 2G \left(\frac{Q}{S} s \right)^{k-1} \Delta T^k \quad (55)$$

$$\boldsymbol{\sigma}^k = \boldsymbol{\sigma}^{k-1} + \Delta \boldsymbol{\sigma}^k \quad (56)$$

And we compute $\Delta \bar{\boldsymbol{\varepsilon}}_p^k$ and update $\bar{\boldsymbol{\varepsilon}}_p^k$:

$$\Delta \bar{\boldsymbol{\varepsilon}}_p^k = \frac{1}{H^k} (\Delta \bar{\boldsymbol{\sigma}}^k + \sqrt{3} \beta^k \Delta T^k) \quad (57)$$

$$\bar{\boldsymbol{\varepsilon}}_p^k = \bar{\boldsymbol{\varepsilon}}_p^{k-1} + \Delta \bar{\boldsymbol{\varepsilon}}_p^k \quad (58)$$

Finally, we compute \mathbf{D}_{ep}^k , \mathbf{Q}^k , \mathbf{S}^k and \mathbf{s}^k for the next-stage computation.

A schematic flowchart for the incremental scheme for the thermo-elastoplastic analysis for FGMs is presented in Fig. 7, where $\Delta \boldsymbol{\sigma}_{Temp}^k$ indicates $\mathbf{D}_{ep}^{k-1} \Delta \boldsymbol{\varepsilon}^k$.

5. Numerical experiments

For the numerical simulation we take a simply supported symmetric plane-stress FGM beam shown in Fig. 8. Its lower surface is kept to be T_0 be 290°K while its upper surface is subjected to a cyclic temperature function $f(t)$ depicted in Fig. 6 with τ_p of 3.0 sec and the peak temperature T_1 of 1190° K. The thermo-mechanical properties of two constituents are listed in Table 1, and the temperature-interval-wise variations of four material properties are contained in Table 2. We note here that linear interpolation is applied to the temperature-dependent properties for obtaining continuous temperature

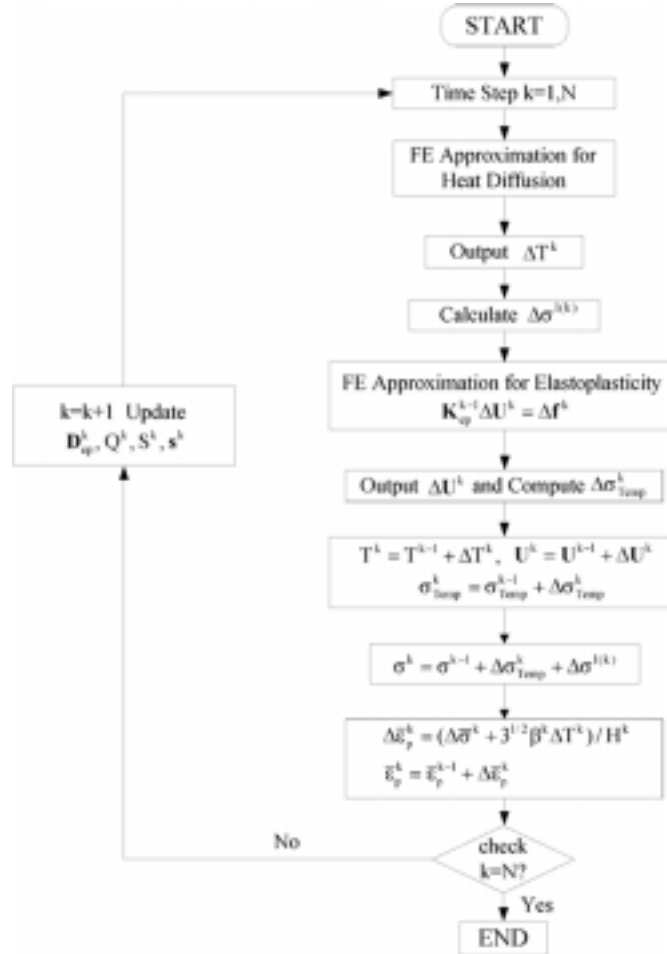


Fig. 7 Flowchart for the incremental thermo-elastoplastic analysis

variations. Sixteen FGM cases (N of 0.5, 1.0, 5.0 and 50 for each χ of 0.2, 0.5, 0.7 and 1.0) together with a CLC are taken for the comparative analysis.

From the symmetry of thermo-elastoplasticity problem with respect to the z -axis, we take a half of the beam for the FEM model. We make 150 uniform partitions along the x -direction, while three layer-wise uniform mesh partitions through the thickness, such that total 13,500 elements are quasi-uniformly constructed, regardless of the choice of two parameters χ and N . According to the theoretical results, we prepared a test FEM program in which two-dimensional isoparametric 8-node quadrilateral elements are employed. By comparing with the numerical solutions given in the paper by Suresh *et al.* (1995), we confirmed its validity.

In accordance with the purpose of this study, we focus on the vertical distributions of thermoelastoplastic behavior through the thickness, which implies that we exclude the edge effect (Williamson *et al.* 1993) that occurs near $x = \pm L/2$ owing to the finite length. To realize such a situation, we impose no temperature gradient on both surfaces at x of $\pm L/2$ and take the numerical results along the z -axis.

Parametric investigation on the thermoelastic characteristics is well presented in the work by Reddy *et al.* (1999), Cho and Oden (2000). In latter a discussion on the choice of suitable time-step size preventing the inherent oscillation in the *Crank-Nicolson-Galerkin* scheme is also described.

In the CLC case, plastic yielding shown in Fig. 9(a) starts from the bottom surface of the N_i -layer and it advances toward the mid-plane (approximately up to z of -3.0 mm). According to the cyclic heating, successive plastic accumulation is observed in the vicinity of the bottom surface. Corresponding thermal stress distributions are shown in Fig. 9(b), where we see the effect associated with the plastic yielding near the bottom surface of the N_i -layer. Despite of the existence of successive plastic yielding near the bottom surface, time-variation in thermal stress distribution is not noticeable. This is because the plastic tangent modulus E_{Tm} in the N_i -layer is significantly smaller compared to E_m and E_c , as listed in Tables 1 and 2.

Fig. 10 shows the results of the χ -FGM family with N of 0.5. Regardless of the relative thickness ratio χ , the plastic yielding occurs in the upper region of graded layer just below the graded- Al_2O_3 interface. It is worth to note that the FGM with χ of 0.2 has the plastic zone near the bottom surface too, and furthermore the plastic response of the FGM with χ of 0.7 as well as one (for χ of 0.2) near the bottom surface is not affected by heating cycle. As χ increases, the peak equivalent plastic strain strictly decreases, except for the f-FGM which has exceptionally high value. Next Figs. 11 and 12 show thermal stress distributions at A, C, E and B, D, respectively. For the f-FGM,

Table 1 Material data of Al_2O_3 and Ni

Properties	Constituents	
	Ni	Al_2O_3
Density (kg/m^3)	8900.0	3970.0
Young's modulus (Gpa)	199.5	393.0
Poisson's ratio	0.3	0.25
Specific heat ($\text{J/kg} \cdot ^\circ\text{K}$)	444.0	775.0
Thermal conductivity ($\text{W/m} \cdot ^\circ\text{K}$)	90.7	30.1
Thermal expansion coefficient ($^\circ\text{K}^{-1} \times 10^{-6}$)	7.44 (293°K)	3.00 (293°K)
	9.89 (1110°K)	5.22 (1110°K)

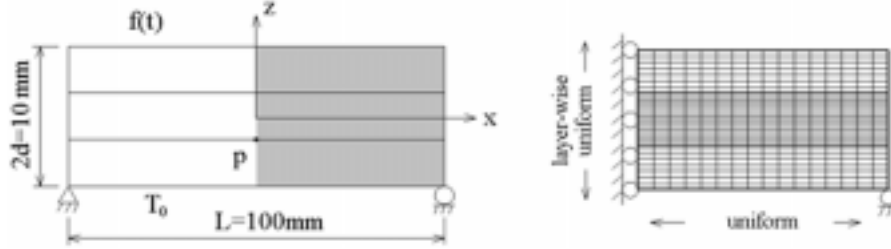


Fig. 8 A plane-stress FGM beam and its finite element model

Table 2 Time-variations in material properties

Temperature (°K)	σ_Y (MPa)	σ_U (MPa)	ϵ_U (%)	E_{Tm} (GPa)
293	148	462	47	0.669
400	153	459	46	0.666
500	140	459	44	0.826
600	138	462	46	0.705
700	115	328	64	0.333
800	100	245	68	0.213
900	69	176	72	0.149
1000	59	121	82	0.076
1100	45	83	95	0.040

considerable time-variation in thermal stress is observed, owing to the existence of large successive plastic yielding. Even though the f-FGM possesses smoother and smaller thermal stress distribution, it has excessive plastic accumulation near the top surface. Hence, in this family, the case of $\chi=0.7$ is more attractive from the thermo-elastoplastic point of view.

Numerical result for the FGMs with N of 1.0 are presented in Figs. 13-15. Compared to the case

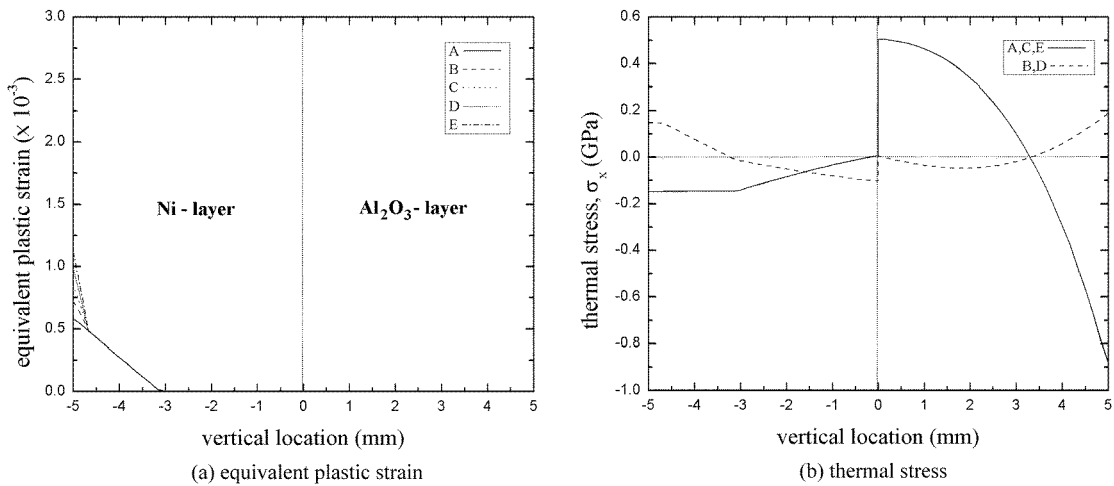


Fig. 9 Thermo-elastoplastic response of CLC

with N of 0.5, the plastic-affected region becomes wider, particularly for the FGMs with χ of 0.5 and 0.7, and the magnitude for the f-FGM becomes significantly smaller, which is caused by the relaxation of the metal volume fraction near the graded- Al_2O_3 interface. The occurrence of plastic zone near the bottom surface up to χ of 0.7 is also remarkable. According to the extension of plastic zone showing successive plastic yielding along heating cycle, for χ of 0.5, 0.7 and 1.0, time-variations of thermal stress in such regions become considerable.

Distributions of the equivalent plastic strain for FGMs with N of 5.0 and 50 are shown in Figs. 16 (when χ is 0.2) and 17 (when χ is 1.0). We first consider the case with N of 5.0. Compared to the previous cases with N of 0.5 and 1.0, we observe that the plastic zone in the graded layer moves down to the Ni -graded interface with a trend of becoming wider and smaller in its magnitude. In addition, the successive plastic accumulation becomes significantly smaller to a negligible extent. This tendency in the graded layer becomes more severe with the increase of χ . On the other hand,

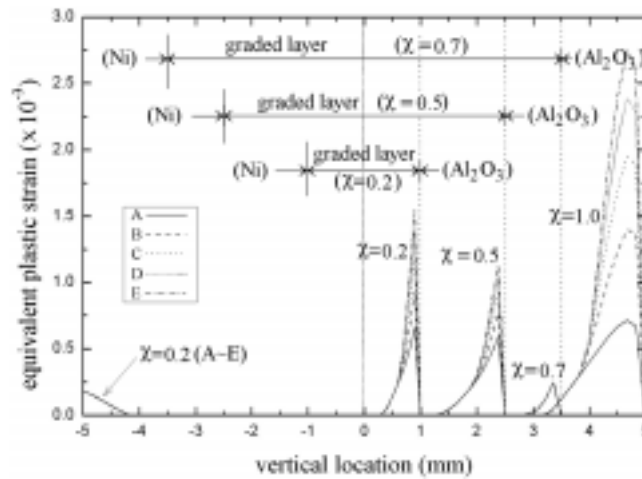


Fig. 10 Distribution of equivalent plastic strain of FGMs with N of 0.5

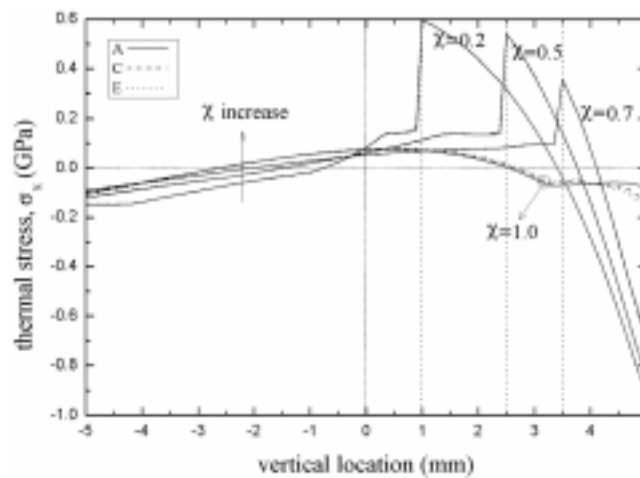


Fig. 11 Thermal stress distributions of FGMs with N of 0.5 at A, C and E

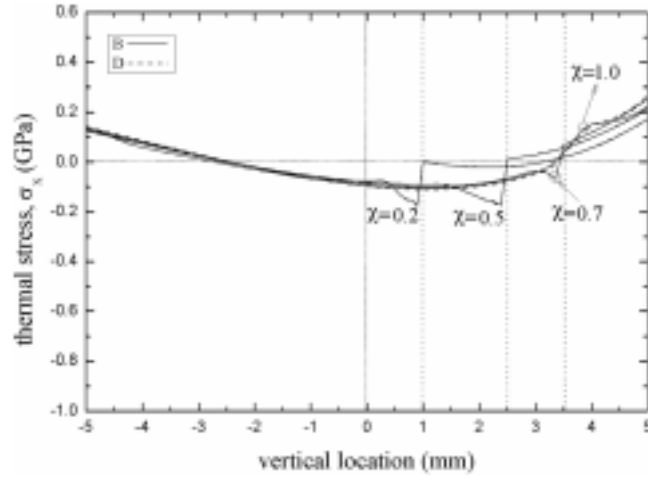


Fig. 12 Thermal stress distributions of FGMs with N of 0.5 at B and D

the plastic zone near the bottom surface becomes wider with the increase in its magnitude. Furthermore, we see more active and sharp increase in successive plastic accumulation, but it does not show a remarkable variation along χ . Since the plastic distribution shows a sequential variation with respect to χ , we exclude the results for the cases with χ of 0.5 and 0.7.

Next, we examine the case with N of 50. From Fig. 16, we see a very small plastic zone extremely moved to the N_i -graded interface, even this tiny plastic zone in the graded layer disappears completely when $\chi \geq 0.5$. According to the increase of χ , the plastic behavior near the bottom surface shows the same trend as the case with N of 0.5, except for the shrinkage of plastic zones.

Corresponding thermal stress distributions for N of 5.0 and 50 are presented in Figs. 18 and 19, respectively. Even though all FGMs with N of 5.0 and 50 experience significant successive plastic yielding near the bottom surface, the f-FGM with N of 50 shows only a noticeable time-variation in

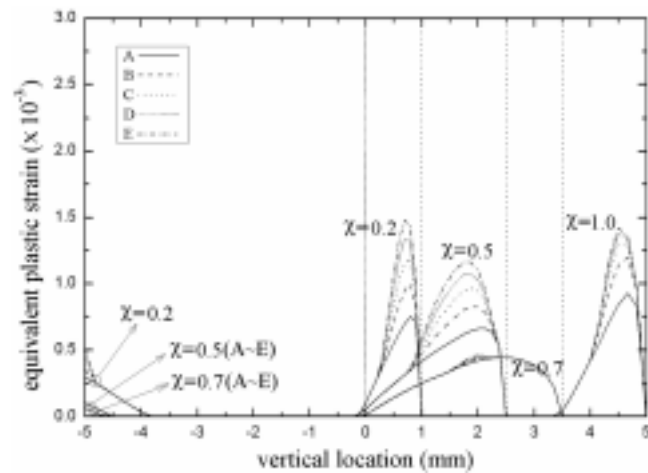


Fig. 13 Distribution of equivalent plastic strain of FGMs with N of 1.0

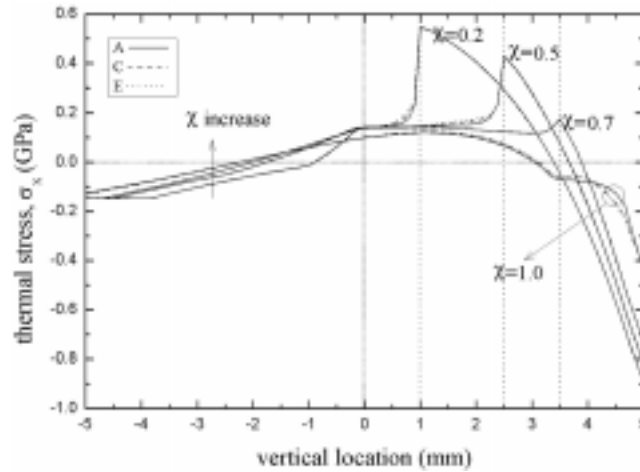


Fig. 14 Thermal stress distributions of FGMs with N of 0.5 at A, C and E

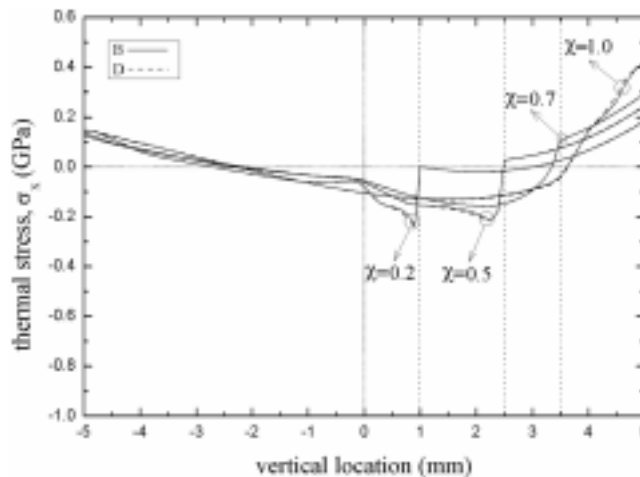


Fig. 15 Thermal stress distributions of FGMs with N of 0.5 at B and D

thermal stress distributions. This is because the Al_2O_3 volume fraction for this case becomes extremely dominated near the bottom surface, as depicted in Fig. 2, which significantly arguments the small plastic tangent modulus of Ni in such a region.

By comparing the whole figures of stress distributions presented so far, we first observe that CLC exhibits the steepest stress jump at layer interface, while the other FGMs exhibit flexible variations according to the choice of two parameters. When N is relatively small ($N \leq 1.0$), except for the f-FGM, considerable stress jumps occur at the graded- Al_2O_3 interface, and which reflects the behavior of m-CLCs. Along the increase of N , thermal stress distributions seem to become smoother but they show again noticeable stress jumps at the Ni -graded interface when N reaches 50, which reflects the behavior of c-CLCs. On the other hand, the f-FGM displays a remarkable stress change near the bottom surface only when N is 50.

Figs. 20(a) and (b) comparatively show total widths of plastic zone in the graded layer and in the

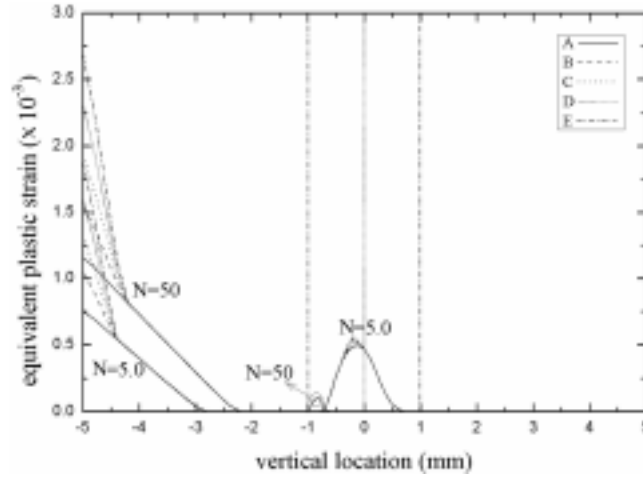


Fig. 16 Distributions of equivalent plastic strain for FGMs with χ of 0.2

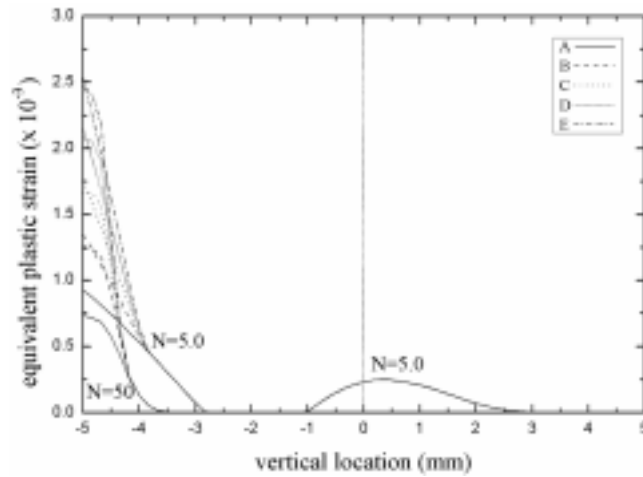


Fig. 17 Distributions of equivalent plastic strain for FGMs with χ of 1.0

Ni -layer, respectively. In the graded layer, the total width becomes larger, as a whole, together with the increase of χ . In addition, for a given χ it reaches the peak when N is 5.0. On the other hand, in the Ni -layer it shows an increase trend as the power index N increases, while it, for relatively high power indices, saturates as χ increases. This figure implies that the plastic region in the graded layer becomes wider as N approaches 5.0 or χ increases, while it, in the Ni -layer, does as N increases.

The plastic zone for each FGM is plotted in Fig. 21(a), where layer interfaces are not indicated because the reader can infer their locations from the value of χ . The plastic zone for χ of 0.2 is splitted into two regions for all values of N . Along the increase of N , one restricted within the region just below the graded- Al_2O_3 interface moves toward the Ni -graded interface, while the other in the Ni -layer just extends toward the Ni -graded interface from the bottom. This tendency of the N -family $M_{0.2}^N$ is because the positive peak thermal stress occurred at the graded- Al_2O_3 interface moves

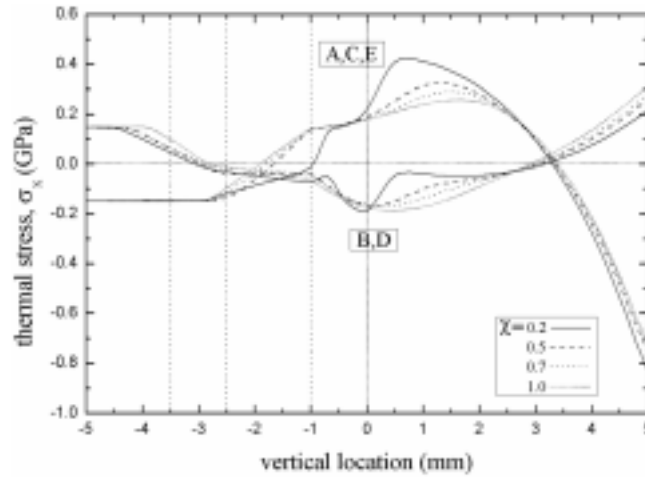


Fig. 18 Thermal stress distributions for FGMs with N of 5.0

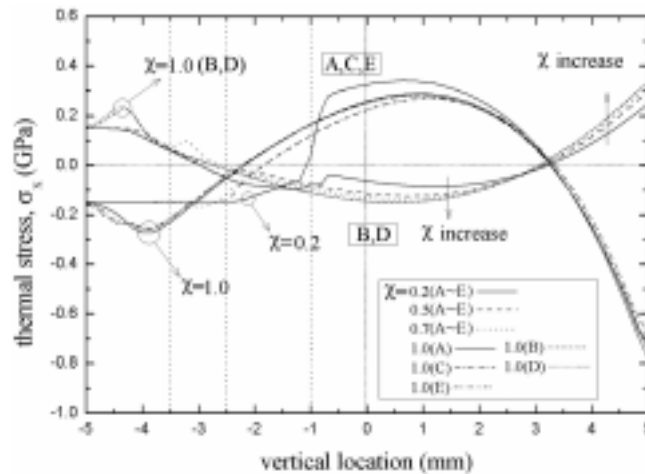


Fig. 19 Thermal stress distributions for FGMs with N of 50

toward the Ni -graded interface and the thermal stress magnitude near the bottom surface increases monotonously, as is well described in our previous work (Cho and Oden 2000).

For the N -families $M_{\chi \geq 0.5}^N$, the trend of plastic zone with respect to the power index N does not show relatively significant difference, except for becoming wider and its complete disappearance when N is 50. On the other hand, plastic zones in the Ni -layer, for N of 5.0 and 50, do not show any noticeable change compared to those of χ with 0.2, but those for $N \leq 1.0$ shrink to zero as χ increases.

Variations in the location of peak equivalent plastic strains, in the graded layer, are shown in Fig. 21(b), where (m) indicates its movement along the heating cycle (*i.e.* $A \rightarrow E$). For each relative thickness ratio χ , the peak position moves from the point just below the graded- Al_2O_3 interface to the Ni -graded interface as N increases. It is worth to note that the FGMs with N of 1.0 experience considerable successive changes in the peak position along the heating cycle.

By examining Figs. (20) and (21), we realize that the equivalent plastic strain distributions in the graded layer becomes more sharp as N approaches zero, regardless of χ . On the other hand, from Figs. (10), (13) and (16)-(17), the variation of its sharpness, in the Ni -layer at time A , with respect to the power index N is not considerable.

Variations of the peak plastic strain in the graded layer and the Ni -layer are shown in Figs. 22(a) and (b), respectively, where the lower one of two curves for each χ is at time A . We first consider Fig. 22(a) for the graded layer. For every N , the peak plastic strain decreases to some extent in proportion of the increase of χ , but it increases when χ approaches unity. On the other hand, the distance between two graphs for each χ , which indicates the magnitude of successive plastic strain accumulation, becomes larger as N decreases.

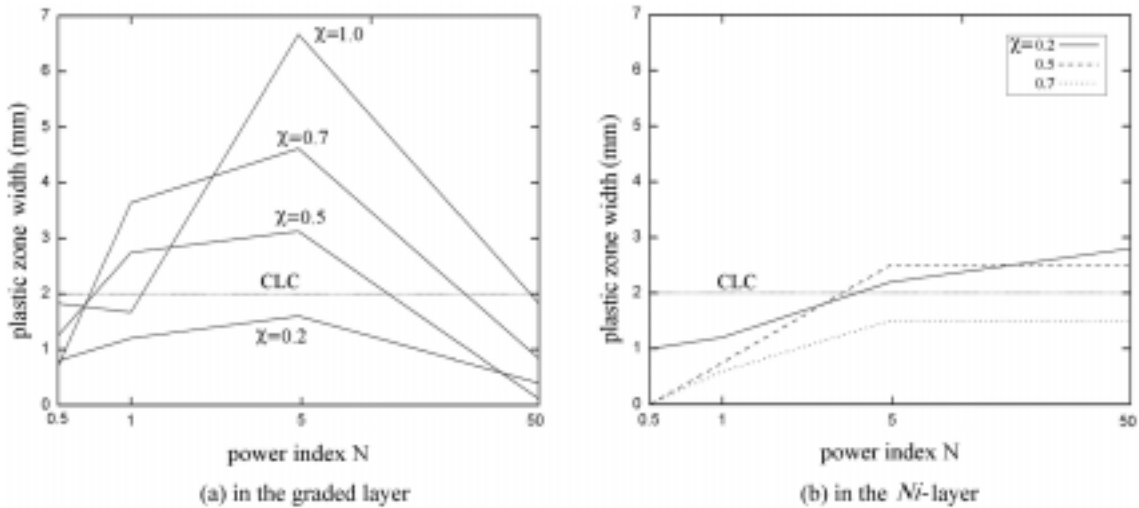


Fig. 20 Variations of the total plastic-zone width

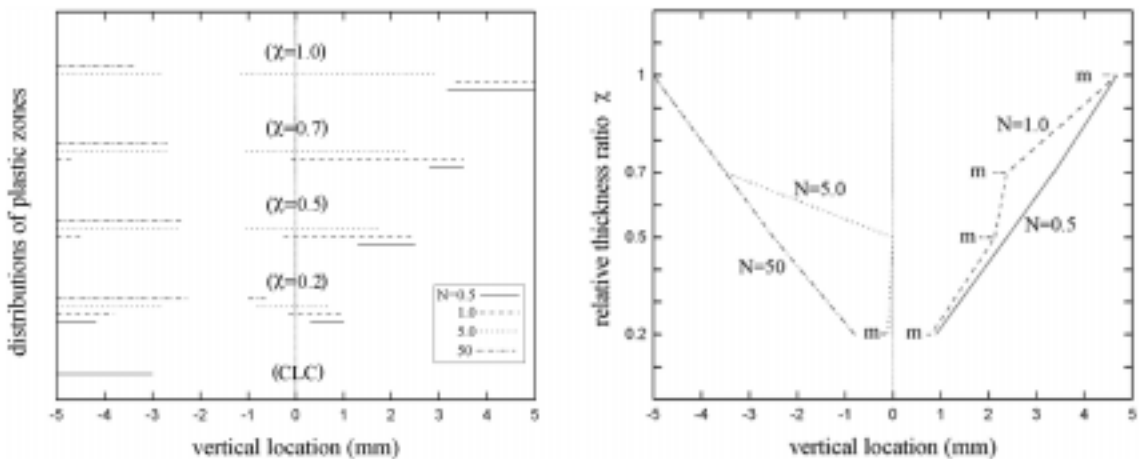


Fig. 21 Distributions of the plastic zone (a) and locations of peak equivalent plastic strain (b), in the graded layer

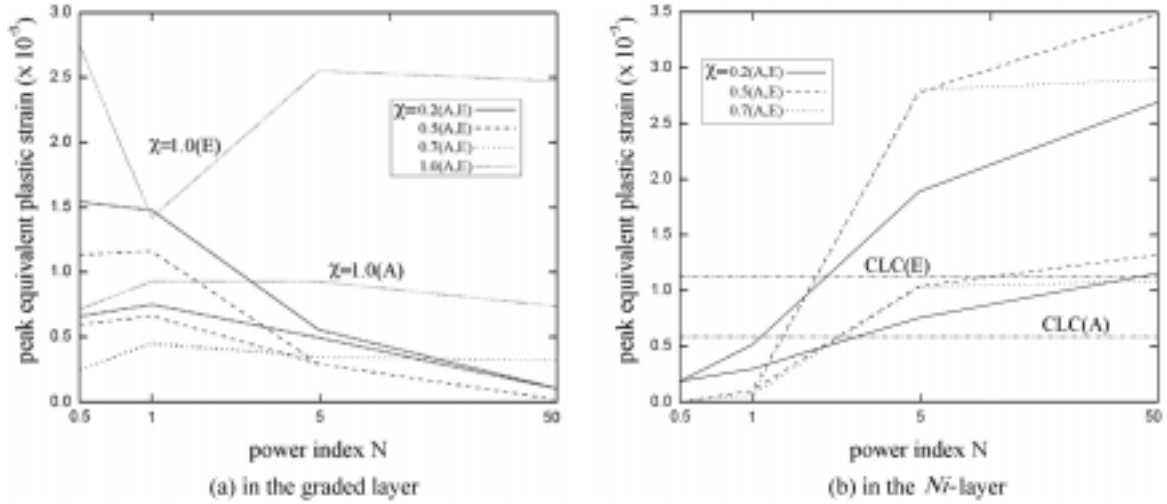


Fig. 22 Variations in the peak equivalent plastic strains at A and E

In the Ni -Layer, FGMs with $N \geq 5.0$ have higher peak values than those of CLC. In addition, for every χ the initial peak plastic strain and the successive plastic accumulation uniformly increase in proportion to the increase of N . In other words, the Ni -layer exhibits higher plastic strain as FGMs approach the c-CLC.

6. Conclusion

In this paper we addressed the parametric investigation on thermo-elastoplastic characteristics of heat-proof functionally graded composites together with the theoretical formulation and the finite element approximations. For the comparative numerical analysis, we selected the volume fraction and the relative thickness ratio of the graded layer as considering parameters. Through the numerical experiments with plane-stress heat-resisting FGM subjected to the heating cycle, we examined the distributions of equivalent plastic strain and thermal stress, and we analyzed the variations associated with the plastic zone, the peak equivalent plastic strain and the successive yielding. According to the investigations through numerical results, the following main observations are drawn.

1. In the graded layer, plastic yielding occurs in the region near the graded- Al_2O_3 interface when N is 0.5, but it moves toward the Ni -graded interface with the trend becoming wider and smoother in proportion to the increase of N . In addition, the total plastic zone width is maximum when N is 5.0 and it shows the increase tendency, according to the extension of the graded layer, but the peak equivalent strain and the distribution sharpness show higher values at lower power index ($N \leq 1.0$). Furthermore, the successive yielding due to heating cycle prevails for χ of 1.0 or smaller N .

2. In the Ni -layer, plastic yielding occurs in the bottom region and the plastic zone advances toward the Ni -graded interface, while showing the saturation behavior, as N increases. In all cases, the peak equivalent plastic strain occurs at the bottom surface, and it shows uniform increase in its magnitude and sharpness in proportion to the increase in N and heating cycle.

3. We also observed that the thermal stress exhibits considerable jumps at the graded- Al_2O_3

interface when N is relatively small, except for the f-FGM, and at the Ni -graded interface when N is 50. However, the stress concentration at the Ni -graded interface is not severe compared to one occurred at the graded- Al_2O_3 interface.

From the numerical results, we observed that a wide range of thermo-elastoplastic characteristics is obtained by varying the combination of two parameters. Thus, this study leads one to the further study on the optimal design of most suitable heat-resisting FGMs for a given purpose, for which one should be able to determine the optimal combination of the volume fraction and the relative thickness ratio.

Acknowledgments

The author (JRC) would like to thank Professor *J. Tinsley Oden* at the University of Texas at Austin for his encouragement on this area of investigation.

References

- Carey, G.F. and Oden, J.T. (1984), *Finite Elements: Computational Aspects*, Vol. III, Prentice-Hall, New Jersey.
- Cho, J.R. and Oden, J.T. (2000), "Functionally graded material: A parametric study on thermal stress characteristics using the Crank-Nicolson-Galerkin scheme", *Comput. Methods Appl. Mech. Engrg.*, **188**, 17-38.
- Cho, J.R. and Ha, D.Y. (2000), "Dual-phase functionally graded composite materials: overall and discrete analysis models", *Key Engrg. Mater.*, **183-187**, 373-378.
- Christensen, R.M. (1979), *Mechanics of Composite Materials*, Wiley-Interscience, New York.
- Giannakopoulos, A.E., Suresh, S., Finot, M. and Olsson, M. (1995), "Elastoplastic analysis of thermal cycling: Layered materials with compositional gradients", *Acta Metall. Mater.*, **43**(4), 1335-1354.
- Hashin, Z. and Shtrikman, S. (1963), "A variational approach to the theory of the elastic behavior of multiphase systems", *J. Mech. Phys. Solids*, **11**, 127-140.
- Hirano, T. and Wakashima, K. (Jan. 1995), "Mathematical modeling and design", *MRS Bulletin*, 40-42.
- Johnson, C. (1990), *Numerical Solution of Partial Differential Equations by the Finite Element Method*, Cambridge University Press, Cambridge.
- Owen, D.R.J. and Hinton, E. (1980), *Finite Elements in Plasticity: Theory and Practice*, Pineridge Press.
- Praveen, G.N., Chin, C.D. and Reddy, J.N. (1999), "Thermoelastic analysis of a functionally graded ceramic-metal cylinder", *ASCE Engrg. Mech.*, **125**(11), 1259-1267.
- Ravichandran, K.S. (1994), "Elastic properties of two-phase composites", *J. Am. Ceram. Soc.*, **77**(5) 1178-1184.
- Reiter, T. and Dvorak, G.J. (1998), "Micromechanical models for graded composite materials. II: Thermo-mechanical loading", *J. Phys. Solids*, **46**(9), 1655-1673.
- Schapery, R.A. (1968), "Thermal expansion coefficients of composite materials", *J. Comp. Mater.*, **2**, 380-404.
- Tomata, Y., Kukori, K., Mori, T. and Tamura, T. (1976), "Tensile deformation of two-ductile-phase alloys: flow curves α - γ Fe-Cr-Ni alloys", *Mater. Sci. Engrg.*, **24**, 85-94.
- Tanaka, K., Tanaka, Y., Enomoto, K., Poterasu, V.F. and Sugano, Y. (1993), "Design of thermoelastic materials using direct sensitivity and optimization methods. Reduction of thermal stresses in functionally gradient materials", *Comput. Methods Appl. Mech. Engrg.*, **106**, 271-284.
- Wakashima, K. and Tsukamoto, H. (1991), "Mean-field micromechanics model and its application to the analysis of thermomechanical behavior of composite materials", *Mater. Science Engrg.*, **A146**, 291-316.
- Yoshitake, A., Tamura, M., Shito, I. and Niino, M. (1990), "Fabrication of the functionally gradient materials (FGM)", The State of Art, *ESA Symposium on Space Application of Advanced Structural Materials*.
- Williamson, R.L., Rabin, B.H. and Drake, J.T. (1993), "Finite element analysis of thermal residual stresses at graded ceramic-metal interfaces. Part 1: Model description and geometrical effects", *J. Appl. Phys.*, **74**(2), 1310-1320.